

Proposal of the new project

# Hadron physics at the COMPASS experiment

within the theme 02-0-1085-2017/2019

Project leader: Guskov A. V.

## Laboratory of Nuclear Problems:

Abazov V. M., Alexeev G. D., Anfimov N. V., Denisenko I. I., Frolov V. N., Gridin A. O., Guskov A. V., Jouravlev N. I., Krumshstein Z. V., Maltsev A. I., Mitrofanov E. O., Olshevski A. G., Orlov I. A., Piskun A. A., Rezinko T. V., Rymbekova A., Tokmenin V. V.

## Laboratory of Theoretical Physics:

Arbuzov A. B.

## Contents

<b>1</b>	<b>Introduction</b>	<b>2</b>
<b>2</b>	<b>COMPASS experiment</b>	<b>3</b>
2.1	COMPASS setup . . . . .	3
2.2	Target zone . . . . .	3
2.3	COMPASS beams . . . . .	4
<b>3</b>	<b>Test of chiral theory predictions</b>	<b>4</b>
3.1	Pion polarizability . . . . .	4
3.2	Kaon polarizability . . . . .	8
3.3	Pion electromagnetic reactions with neutral pions in the final state . . . . .	8
<b>4</b>	<b>Exotic charmonia</b>	<b>9</b>
4.1	Exclusive leptoproduction of exotic charmonia . . . . .	9
4.2	Exclusive production of pentaquarks $P_c^+(4380)$ and $P_c^+(4450)$ . . . . .	12
4.3	Pion-induced exclusive production of the $Z_c^-(3900)$ state off a nuclear target . . . . .	12
<b>5</b>	<b>Study of the EMC effect in the pion-induced Drell-Yan process</b>	<b>14</b>
<b>6</b>	<b>Preparation of future physics program</b>	<b>15</b>
6.1	Test of chiral theory with kaon beam . . . . .	16

6.2 Prompt photons . . . . .	16
<b>7 Preparation of the detector upgrade</b>	<b>18</b>
<b>8 Plan for JINR group to 2017-2019</b>	<b>18</b>
<b>9 Estimation of cost and resources</b>	<b>19</b>

## 1 Introduction

Despite the success of numerous experiments with colliding beams which certainly bring us to the frontier of particle physics, they have not been able to fully replace experiments with a fixed target. The luminosity that can be reached in the beam–target interactions is many orders of magnitude higher than the luminosities reached by colliders. Fixed-target experiments provide a unique possibility to operate with beams of unstable particles, such as muons, pions and kaons. Studying particle interactions with different nuclei is also much simpler with a fixed target. Therefore, fixed-target experiments remain important instruments in particle physics for center-of-mass energies below 50 GeV.

COMPASS [1] is a fixed-target experiment at a secondary beam of the Super Proton Synchrotron at CERN. The purpose of this experiment is the study of hadron structure and hadron spectroscopy with muon and hadron beams of high intensity. The experiment has an intensive physics programme which includes such topics as:

- study of unpolarized and polarized structure of nucleon using semi-inclusive deep inelastic scattering, Drell-Yan process (DY) and Deeply-Virtual Compton Scattering (DVCS) (**not a part of this Project, see the project 02-0-1085-2017/2019 [2]**);
- study of properties of hadronic interaction (including tests of the chiral theory predictions using energetic pion and kaon beams) and search for new hadron states in diffractive, central, Primakoff and lepto(photo)-production.

In addition to the physics tasks existing for a long time and mentioned in the Proposal of the phase II [3], new tasks appeared recently. Some of these tasks like search for lepto(photo)production of exotic charmonia (introduced by JINR group) and study of the EMC-effect in the pion-induced Drell-Yan process, are mentioned below as the subjects of our interest.

At the moment the second phase of the experiment [3], approved at CERN till the end of 2017, is under realization. Nevertheless, the COMPASS collaboration discusses the physics program for the period after 2020 and the upgrade of the experimental setup related with this program. Importance of the future program with hadron beams was emphasized at the "Physics Beyond Colliders Kickoff Workshop" at CERN (Sep. 6-7, 2016) [4]. For wide discussion of the future COMPASS program the workshop "COMPASS beyond 2020" is scheduled for March next year. We ask to approve participation of the JINR group in **the new project "Hadron physics at the COMPASS experiment"** for the period 2017-2019, where the planned activities are: participation in the data analysis, participation in the data taking, preparation of the proposal for the future physics program and detector upgrade.

## 2 COMPASS experiment

### 2.1 COMPASS setup

The COMPASS setup can be divided into four parts along the beam axis. It starts with the beam line telescope and the detectors that identify the incoming beam particles. It is followed by the target region, which is specific for each of the COMPASS physics programmes. It includes the target and the detectors located in its vicinity (see 2.2). The third part called the Large Angle Spectrometer (LAS) is built around the first dipole magnet SM1. The fourth part is the Small Angle Spectrometer (SAS), which occupies the downstream part of the setup.

The beam part of the setup includes the Beam Momentum Station (BMS), the spectrometer based on an analysis magnet and tracking detectors, which measures the momentum of the incoming muon on an event-by-event base. The BMS is not used with a hadron beam. A precise track reconstruction of the incident particle is provided by fast trackers located upstream of the target. Scintillator veto counters define the beam spot size.

The large angle spectrometer includes the detectors located both upstream and downstream of the SM1 magnet. The LAS detects scattered particles with polar angles of up to 180 mrad. The SM1 magnet is followed by a RICH detector which is used to identify charged hadrons with momenta ranging from a few GeV/c to 43 GeV/c. The LAS is completed by an electromagnetic calorimeter ECAL1 and a hadron calorimeter HCAL1 with a central hole matching the second spectrometer acceptance. A muon filter (muon wall 1, MW1), based on the Mini Drift Tube detectors, is placed at the end of the LAS.

The last part of the COMPASS setup, the Small Angle Spectrometer, detects particles at small angles (less than 30 mrad) and large momenta of 5 GeV/c and higher. Its central element is the SM2 magnet located 18 m downstream of the target centre and preceded and followed by the telescopes of the trackers. The LAS is completed by a set of electromagnetic and hadron calorimeters ECAL2 and HCAL2 and the second muon filter (muon wall 2, MW2).

### 2.2 Target zone

The target region for the muon programme is occupied by the cryogenic  ${}^6\text{LiD}$  (2002–2006) and  $\text{NH}_3$  (2007–2011) targets subdivided into two (2002–2004) and three (2006–2011) cylindrical cells placed along the beam direction. The target material of each individual cell was longitudinally or transversely polarized.

A liquid hydrogen target was mainly used for data taking with hadron beam in 2008 and 2009. The target is surrounded by a time-of-flight Recoil Proton Detector (RPD). Precise silicon tracking detectors are installed up- and downstream of the target. In 2009 and 2012 the liquid hydrogen target was removed and replaced with a specially designed solid-target holder where up to 16 solid targets with different atomic numbers and different thicknesses were mounted. Nickel, carbon, tungsten and lead targets were used (see Tab. 2).

A two-cell polarized ammonia target (55 mm + 55 mm) was used in 2014 and 2015 for the Drell-Yan data taking with a negative pion beam [7]. In order to reduce occupancy of downstream detectors a thick hadron absorber made of aluminium, alumina ( $\text{Al}_2\text{O}_3$ ) and stainless steel was placed immediately downstream the polarized target. The inner part of the absorber contains a tungsten beam plug which can also be treated as an additional target. A small aluminium target was also installed in front of the

Table 1: Relative composition of the hadron beam at the COMPASS target for 190 GeV/c

Particles	Positive beam	Negative beam
$\pi$	0.240	0.968
K	0.014	0.024
p	0.746	0.008

beam plug.

For the data taking within the framework of the GPD programme, in 2016 and 2017 a 2.5-meter long liquid hydrogen target will be used [8]. To measure and identify the recoil proton, a 4-meter long time-of-flight detector called CAMERA is surrounding the target. A large angle electromagnetic calorimeter ECAL0 with aperture of about 0.2-0.6 rad is also added.

### 2.3 COMPASS beams

Secondary negative and positive muon and hadron beams, produced by 400 GeV/c protons from the CERN SPS at a primary production target can be extracted to the COMPASS target. Positive muons of 160 GeV/c (2002-2007, 2010) and 200 GeV/c (2011) with an intensity of up to  $4 \times 10^7 s^{-1}$  were used for the COMPASS muon programme. A negative muon beam of 190 GeV/c was used in 2009 and 2012 for pion polarizability measurement as a reference. Positive and negative muon beams of 160 GeV/c will be used for the GPD programme (2016-2017).

A negative hadron beam of 190 GeV/c mainly composed of pions, was used for data taking in 2008, 2009 and 2012 hadron runs as well as for the Drell-Yan programme in 2014-2015. Measurements with a positive 190 GeV/c hadron beam, mainly composed of protons, were also performed in 2008. The nominal intensity of the hadron beams was  $5 \times 10^6 s^{-1}$  (up to  $2 \times 10^7 s^{-1}$  for Drell-Yan measurements). The particle composition of the hadron component of the beam is given in Tab. 1. It does not include the muon component, which is present on the level of about 1% and negligibly small admixture of electrons and positrons.

Two Cherenkov detectors, CEDARs, are installed 30 m before the COMPASS target region. They were designed to provide fast beam particle identification at high rates for particle momenta of up to 300 GeV/c. They are mainly used for kaon/pion separation.

The full list of data sets collected by COMPASS is presented in Tab. 2. Large number of different combinations of beams and targets makes COMPASS a unique instrument for the hadron spectroscopy and study of the hadronic interactions.

## 3 Test of chiral theory predictions

### 3.1 Pion polarizability

In classical physics the polarizability of a medium or a composite system is a well-known characteristic related to the response of the system to the presence of an external electromagnetic field. If we consider a dipole, the electric polarizability  $\alpha$  is the proportionality constant between the electric field and the electric

Table 2: Data sets collected by COMPASS

Year	Target	Beam particle	Beam momentum, GeV/c
2002	${}^6\text{LiD}$	$\mu^+$	160
2003	${}^6\text{LiD}$	$\mu^+$	160
2004	${}^6\text{LiD}$	$\mu^+$	160
2006	${}^6\text{LiD}$	$\mu^+$	160
2007	$\text{NH}_3$	$\mu^+$	160
2008	Liquid $\text{H}_2$	$\pi^-, K^-$	190
2009	Liquid $\text{H}_2$ , Ni, W, Pb	$\pi^-, K^-, \mu^-$	190
2010	$\text{NH}_3$	$\mu^+$	160
2011	$\text{NH}_3$	$\mu^+$	200
2012	Ni, C, W, Pb	$\pi^-, K^-, \mu^-$	190
2014	$\text{NH}_3$ , W, Al	$\pi^-$	190
2015	$\text{NH}_3$ , W, Al	$\pi^-$	190
2016	Liquid $\text{H}_2$	$\mu^\pm$	160
2017	Liquid $\text{H}_2$	$\mu^\pm$	160 (planned)

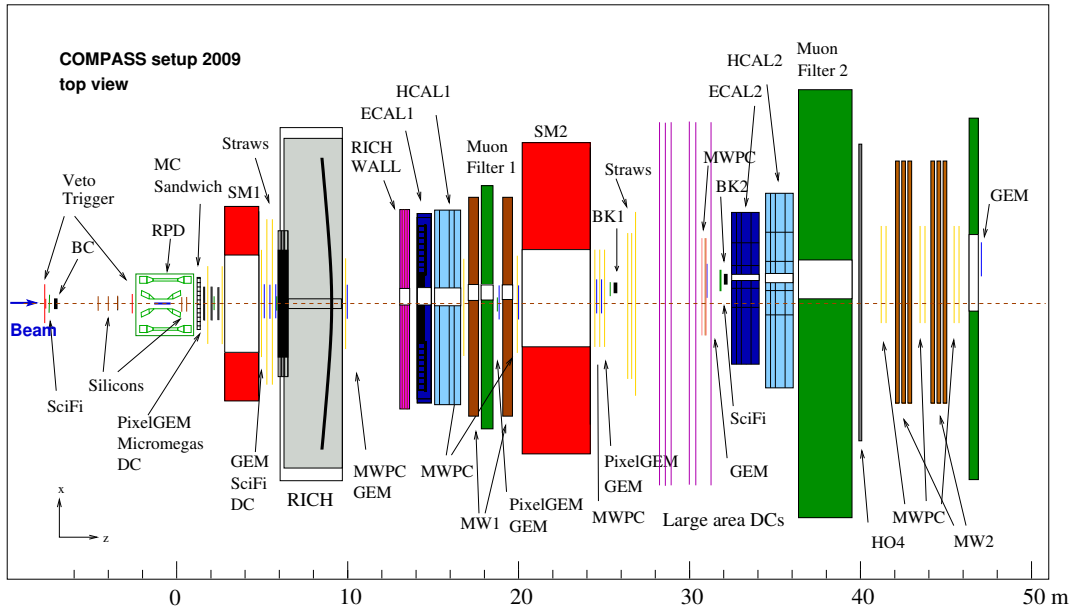


Figure 1: Top view of the COMPASS setup for data taking with hadron beams in 2009 [6]

dipole moment, while  $\beta$  is related to the magnetic field and the magnetic dipole moment. This concept can be extended up to the case of such composite particles as hadrons. In this case the electric polarizability  $\alpha$  and the magnetic polarizability  $\beta$  describe the rigidity of such objects against the deformation by the external electric and magnetic fields and can be tested in the reaction of Compton scattering off hadrons. They are fundamental characteristics of hadrons and the comparison of the theoretically predicted and directly measured values provides a stringent test of various theoretical models in the low-energy region.

Several attempts to measure the pion electric ( $\alpha_\pi$ ) and magnetic ( $\beta_\pi$ ) polarizabilities in the dedicated experiments were performed. The groundbreaking work at Serpukhov [9, 10] used the Primakoff-like process of pion radiative scattering off the nuclear target (Fig. 11 (left))

$$\pi^-(A, Z) \rightarrow \pi^-(A, Z)\gamma. \quad (1)$$

Pion photoproduction  $\gamma p \rightarrow n\pi^+$  was used to determine the pion polarizabilities at Lebedev Institute [11] and MAMI [12]. Certain results were also obtained using the reaction  $\gamma\gamma \rightarrow \pi^+\pi^-$  in  $e^+e^-$  collisions [13–16, 18, 19]. The experimental values for the quantity  $\alpha_\pi - \beta_\pi$  assuming  $\alpha_\pi + \beta_\pi = 0$  are shown in Fig. 2 (right) [21]. These obtained results were affected by large statistical and systematic uncertainties and their accuracy was a few times lower than the precision of theoretical predictions.

The Chiral Perturbation Theory (ChPT), the most successful model in the low-energy region, predicts for the charged pion in the two-loop approximation the values  $\alpha_\pi - \beta_\pi = (5.7 \pm 1.0) \times 10^{-4} fm^3$  and  $\alpha_\pi + \beta_\pi = 0.16 \times 10^{-4} fm^3$  [20]. Basing on the recent precise measurement of the pion weak form factors by the PIBETA collaboration [23] one finds  $\alpha_\pi = -\beta_\pi = (2.78 \pm 0.10) \times 10^{-4} fm^3$ .

There are calculations of the pion polarizabilities in many other models: linear  $\sigma$ -model with quarks [24], chiral quark model [25], super-conductor quark model [26], quark confinement model [27], dispersion relations [28, 29], lattice QCD [30], etc. But almost all of them predict the value of the electric polarizability  $\alpha_\pi$  within the range  $3.5 \times 10^{-4} fm^3 < \alpha_\pi < 7.0 \times 10^{-4} fm^3$  [31], larger than ChPT predicts. More detailed reviews of the present status of this matter can be found in [32, 33].

The reaction (1) is used to measure the pion polarizabilities at COMPASS. It can be treated as Compton scattering of a virtual photon, provided by a target nucleus, off the pion. The 4-momentum transferred to the nucleus in the reaction is very small ( $Q \ll m_\pi/c$ ). In the center-of-mass system the differential cross section can be described by the formula [22, 34]:

$$\frac{d^3\sigma_{\pi(A,Z)}}{dsdQ^2d\Omega} = \frac{\alpha Z^2}{\pi(s - m_\pi^2)} \frac{Q^2 - Q_{min}^2}{Q^4} F^2(Q^2) \times \frac{d\sigma_{\pi\gamma}}{d\Omega} \quad (2)$$

where  $m_\pi$  is the pion mass,  $\alpha$  is the fine structure constant,  $s$  is the squared total energy of the  $\pi\gamma$  system,  $Q_{min}^2 = (s - m_\pi^2)^2/4E_0^2$ ,  $F(Q^2) \approx 1$  is the electromagnetic form factor of the nucleus,  $d\Phi$  is a phase-space element of the final-state and

$$\frac{d\sigma_{\pi\gamma}}{d\Omega} = \left( \frac{d\sigma_{\pi\gamma}}{d\Omega} \right)_0 - \frac{\alpha m_\pi^3 (s - m_\pi^2)^2}{4s^2 (s z_+ + m_\pi^2 z_-)} \left( z_-^2 (\alpha_\pi - \beta_\pi) + \frac{s^2}{m_\pi^4} z_+^2 (\alpha_\pi + \beta_\pi) \right). \quad (3)$$

Here  $z_\pm = 1 \pm \cos\theta$ , where  $\theta$  is the  $\pi\gamma$  scattering angle. Thus the cross section depends on  $\alpha_\pi + \beta_\pi$  at forward angles and on  $\alpha_\pi - \beta_\pi$  at backward angles. Consequently, pion polarizabilities  $\alpha_\pi$  and  $\beta_\pi$  can be accessed via precise measurement of energy and angular distributions of produced photons and their comparison with the expectations for the point-like pion.

In 2015 COMPASS published the first result for the pion polarizabilities. It was obtained using the data collected in 2009 with a negative pion beam of 190 GeV/c and a nickel target [22]. The number of

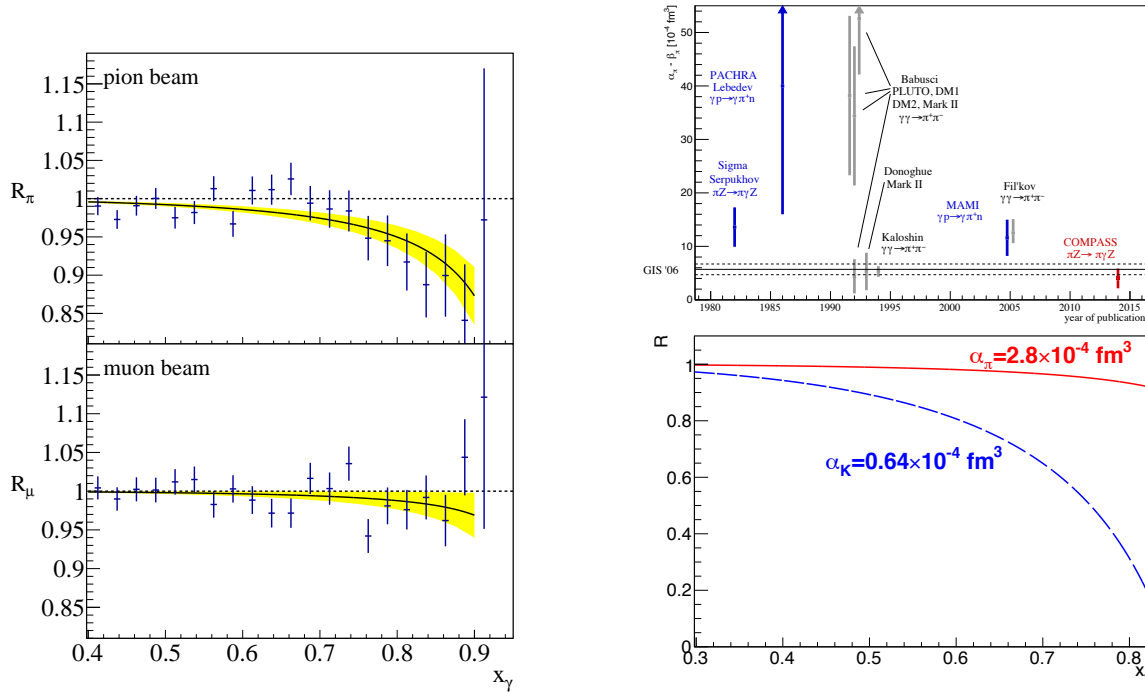


Figure 2: Ratios  $R_\pi$  and  $R_\mu$  of the measured differential cross sections over the expected cross sections for the point-like pion and muon as functions  $x_\gamma$  [22] (left). Experimental results for the quantity  $\alpha_\pi - \beta_\pi$  assuming  $\alpha_\pi + \beta_\pi = 0$  [21]. Horizontal lines represent the prediction of ChPT [20] (right, top). Ratio  $R$  of the differential cross sections for the pion with polarizability  $\alpha_\pi = 2.8 \times 10^{-4} \text{ fm}^3$  and the kaon with polarizability  $\alpha_K = 0.64 \times 10^{-4} \text{ fm}^3$  to the corresponding cross sections for the point-like pion and kaon (right, bottom)

collected  $\pi\gamma$  events with a photon energy above 76 GeV is 63 000. A comparable data sample with a negative muon beam of the same momentum was also collected. Since the muon is a point-like particle, the measured differential cross section should exactly correspond the QED calculations. This muon sample was used to control the possible systematic effects. The ratios  $R_\pi$  and  $R_\mu$  of the measured differential cross sections over the expected cross sections for the point-like pion and muon as a function of the energy of emitted photon normalized to the beam energy  $x_\gamma$  are shown in Fig. 2 (left). The resulting value  $\alpha_\pi = (2.0 \pm 0.6_{stat} \pm 0.7_{syst}) \times 10^{-4} \text{ fm}^3$  was determined assuming  $\alpha_\pi + \beta_\pi = 0$  from the fit of the function

$$f(x_\gamma) = 1 - \frac{3}{2} \frac{m_\pi^3}{\alpha} \frac{x_\gamma^2}{1 - x_\gamma} \alpha_\pi \quad (4)$$

to  $R_\pi$ . The measured ratio  $R_\mu$  is consistent with the hypothesis of the point-like structureless muon. The obtained result for the pion polarizability is at significant variance with the previous experiments and compatible with the expectation from ChPT. The COMPASS measurement is the most precise dedicated measurement of this value at the moment (see Fig. 2 (right)). This result is included as the first entree to the PDG 2016 issue [35].

Nevertheless, the uncertainty of the present result is still much larger than the accuracy of the ChPT prediction. A new set of data collected at COMPASS during the hadron run 2012 with a few times larger statistics is under analysis. The statistics in the control sample collected with a muon beam in 2012 was

also increased. Therefore, one can expect reduction of both statistical and systematic uncertainties of the new result for  $\alpha_\pi$  under assumption  $\alpha_\pi + \beta_\pi = 0$ . The new data cover a larger range of the photon energy in respect to 2009, down to about 20 GeV, that is especially important for independent measurement of  $\alpha_\pi$  and  $\beta_\pi$ .

### 3.2 Kaon polarizability

Since the kaon is a more compact and rigid object than the pion, it would be natural to expect smaller values for kaon polarizabilities. The prediction of the chiral perturbation states that, for the charged kaon, the polarizability is  $\alpha_K = (0.64 \pm 0.10) \times 10^{-4} fm^3$  under assumption that  $\alpha_K + \beta_K = 0$  [36]. While the prediction of the quark confinement model is rather different:  $\alpha_K = 2.3 \times 10^{-4} fm^3$ ,  $\alpha_K + \beta_K = 1.0 \times 10^{-4} fm^3$  [27]. As for the experimental results, only the upper limit  $\alpha_K < 200 \times 10^{-4} fm^3$  (CL=90%) has been established from the analysis of X-rays spectra of kaonic atoms [37]. The reaction

$$K^-(A, Z) \rightarrow K^-(A, Z)\gamma. \quad (5)$$

can be used to determine the kaon polarizability. The expected ratio  $R$  for the kaon with polarizability  $\alpha_K = 0.6 \times 10^{-4} fm^3$  and for the pion with polarizability  $\alpha_\pi = 2.8 \times 10^{-4} fm^3$  as a function of  $x_\gamma$  is depicted in Fig. ?? (left). Despite small contamination of kaons in the beam and low cross section of the reaction (5) (proportional to  $m^{-2}$ ) COMPASS provides unique possibility to touch this quantity.

### 3.3 Pion electromagnetic reactions with neutral pions in the final state

In parallel to the pion and kaon polarizabilities measurements COMPASS also aims to study low  $Q^2$  electromagnetic reactions with neutral mesons in the final state:

$$\pi^-(A, Z) \rightarrow \pi^-(A, Z) \pi^0, \quad (6)$$

$$\pi^-(A, Z) \rightarrow \pi^-(A, Z) \pi^+\pi^-, \quad (7)$$

$$\pi^-(A, Z) \rightarrow \pi^-(A, Z) \pi^0\pi^0, \quad (8)$$

The measurement of Eq. (6) allows determining the chiral anomaly amplitude  $F_{3\pi}$ , for which the ChPT makes an accurate prediction by relating the process to the  $\pi^0$  decay constant  $F_\pi$  [38]:

$$F_{3\pi}(s = 0, t = 0, Q^2 = 0) = \frac{F_\pi}{f^2\sqrt{4\pi\alpha}}, \quad (9)$$

where  $f$  is the the charged pion decay constant. This constitutes a test of a higher-order ChPT predictions. The Reaction has already been examined at the SYGMA spectrometer (Serpukhov) [39], however in the relevant region of  $s < 10m_\pi^2$  only about 200 events were found. The constant of the similar reaction with  $\eta$ -meson in the final state has been also tested in VES [42] with low precision.

The cross sections of the reactions (7) and (8), which are governed by the chiral  $\pi\pi$ -interaction, calculated as functions of the center-of-mass energy  $\sqrt{s}$  at the tree level in [40], are shown in Fig. 3(left). Here, the ChPT expansion should be reliable on the percent level, and thus, the experiment would constitute a strong test of ChPT at the tree level and much beyond the determination of low-energy constants. The cross section of the reaction (7) has already been measured as a function of  $\sqrt{s}$  by COMPASS [41] and is in good agreement with the ChPT prediction as it is shown in Fig. 3(right).

Similar kaon-induced reactions can also be tested in COMPASS.

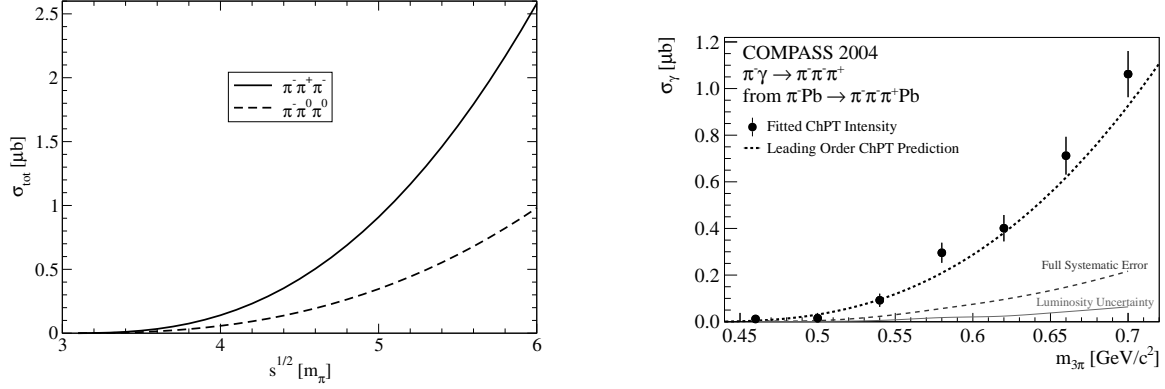


Figure 3: Total cross sections for the reactions (7) and (8) as a function of the total center-of-mass energy  $\sqrt{s}$  (left) [40]. Cross section of the reaction (7) measured by COMPASS [41]

## 4 Exotic charmonia

The first unexpected charmonium state contradicting to the quark model was the X(3872) observed by Belle [43] in 2003 in the decay  $B^+ \rightarrow J/\psi K^+ \pi^+ \pi^-$ . With the experimental progress, the family of the charmonium-like states has become more and more abundant. To date, dozens of charmonium- and bottomonium-like states, the so-called XYZ states, have been observed in numerous reaction channels and final states, such as  $e^+e^-$  collisions by CLEO-c, BaBar, Belle, BESIII and in hadronic interactions by CDF, D0, LHCb, CMS, and ATLAS. Several interpretations of the new states do exist: pure quarkonia, tetraquarks, hadronic molecules, hybrid mesons with a gluon content, etc. But at the moment many basic parameters of XYZ states have not been determined yet. New experimental input is required to distinguish between the models that provide different interpretations of the nature of these states. COMPASS has a unique possibility to contribute to XYZ physics by investigating lepto(photo)production of these states.

The review of the present situation in the XYZ physics can be found in [44, 45].

Despite hadron spectroscopy is old and one of the main topics of the COMPASS physics program, the most of analyses are concentrated on the spectroscopy of light hadrons. The spectroscopy of exotic charmonia was introduced to COMPASS by the JINR in 2013 and is the matter of its particular interest.

### 4.1 Exclusive lepto-production of exotic charmonia

The COMPASS setup and the COMPASS kinematics are suitable for study of exclusive production of charmonia. On the one hand, the center-of-mass energy  $\sqrt{s} = (17.3 - 19.4) \text{ GeV}$  is high enough to produce a number of interesting final states, on the other hand, the excellent tracking system and the electromagnetic calorimeters provide strict control of exclusivity.

Photoproduction of exotic charmonia off a proton in the charge exchange and the neutral exchange

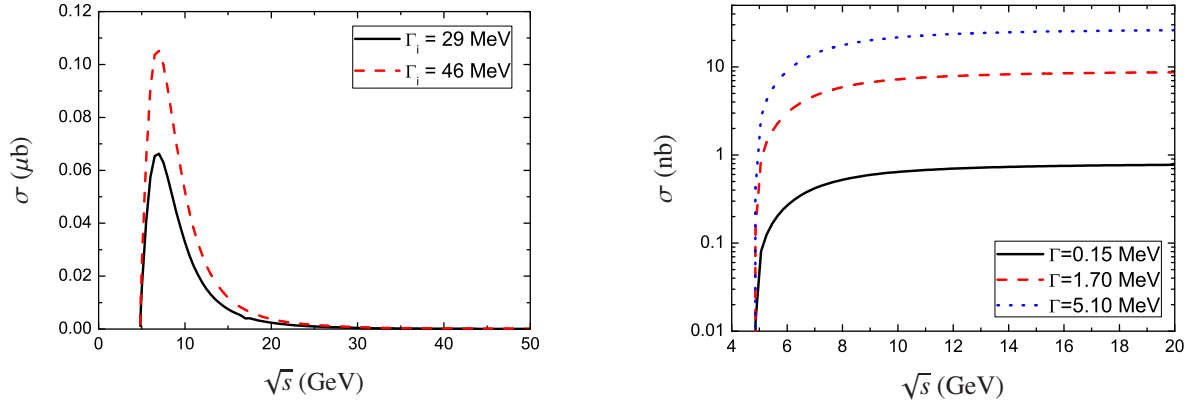


Figure 4: Total cross section for the charge exchange reaction (13) (left) [49] and the neutral exchange reaction [] (right) as a function of the center-of-mass energy of  $\gamma N$  system shown for the different widths of the produced  $Z^+(3900)$  and  $Y(3940)$  states

reactions is discussed in a series of papers:

$$\gamma p \rightarrow Z_c^+(4430)n \rightarrow \psi(2S)\pi^+n \quad [46], \quad (10)$$

$$\gamma p \rightarrow Y(3940)p \quad [47], \quad (11)$$

$$\gamma p \rightarrow X(3915)p \rightarrow J/\psi\omega p \quad [48], \quad (12)$$

$$\gamma p \rightarrow Z_c^+(3900)n \quad [49], \quad (13)$$

$$\gamma p \rightarrow Z_c^+(4360)n \quad [50]. \quad (14)$$

The energy dependence of the total cross sections exhibits a strong threshold enhancement for the charge exchange channels, while for the neutral exchange the cross section goes on a plateau that makes their study convenient using a source of virtual or real energetic photons. Such dependences are presented as an example at the left and right panels of Fig. 4, respectively. The obtained results can be transposed to the case of leptonproduction off a nucleon.

Exclusive leptonproduction of the hadron  $Z_c^\pm(3900)$ , which is the most probable candidate to be a tetraquark, has been searched for at COMPASS [51] in the reaction

$$\mu^+ N \rightarrow \mu^+ Z_c^\pm(3900)N' \rightarrow \mu^+ J/\psi\pi^\pm N' \rightarrow \mu^+ \mu^+ \mu^- \pi^\pm N' \quad (15)$$

using the full set of muon data collected in 2002-2011. According to the vector meson dominance (VMD) model, a photon may behave like a  $J/\psi$  so that a  $Z_c^\pm(3900)$  can be produced by the interaction of the incoming virtual photon, emitted by the incoming muon with a virtual charged pion provided by the target nucleon.

The mass spectrum for  $J/\psi\pi^\pm$  events is shown in Fig. 5 (left). It does not exhibit any statistically significant signal around the nominal mass of  $Z_c(3900)$ . The upper limit of the  $Z_c(3900)$  production rate was established to be

$$BR(Z_c^\pm(3900) \rightarrow J/\psi\pi^\pm) \times \sigma_{\gamma N \rightarrow Z_c^\pm(3900)N} \Big|_{\langle \sqrt{s_{\gamma N}} \rangle = 13.8 \text{ GeV}} < 52 \text{ pb}, \quad (CL = 90\%). \quad (16)$$

The result is included to the PDG review [35].

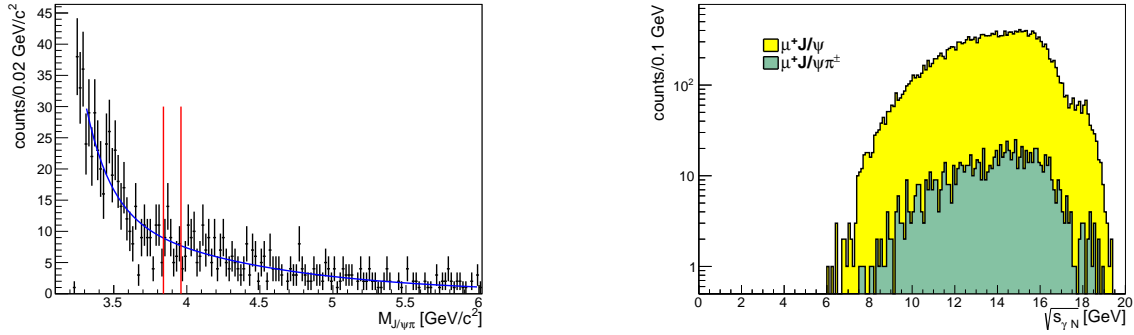


Figure 5: Mass spectrum of the  $J/\psi\pi^\pm$  state [51] (left).  $\sqrt{s_{\gamma N}}$  distribution for exclusive  $\mu^+J/\psi$  and  $\mu^+J/\psi\pi^\pm$  events [51] (right)

Another promising reaction is the charge exchange process

$$\mu^+ N \rightarrow \mu^+ X^0 \pi^\pm N' \rightarrow \mu^+ (J/\psi \pi^+ \pi^-) \pi^\pm N' \rightarrow \mu^+ (\mu^+ \mu^- \pi^+ \pi^-) \pi^\pm N', \quad (17)$$

where  $X^0$  is the well-known charmonium  $\psi(2S)$  or the exotic state  $X(3872)$ . A possible model for the production process is shown in Fig. and can be derived by using the VMD model and by crossing the decay diagram for  $X^0 \rightarrow J/\psi \pi^+ \pi^-$ . In case of the same production mechanism for  $X(3872)$  and  $\psi(2S)$  and neglect the difference in kinematics of their production and decay caused by the mass difference one can derive the relation

$$\frac{N_{X(3872)}}{N_{\psi(2S)}} = \frac{\Gamma_{X(3872) \rightarrow J/\psi \pi \pi}^2 \times \Gamma_{\psi(2S)}}{\Gamma_{\psi(2S) \rightarrow J/\psi \pi \pi}^2 \times \Gamma_{X(3872)}}, \quad (18)$$

where  $N_{X(3872)}$  and  $N_{\psi(2S)}$  are the numbers of events, produced according to the diagram in Fig 6(left),  $\Gamma_{X(3872) \rightarrow J/\psi \pi \pi}$  and  $\Gamma_{\psi(2S) \rightarrow J/\psi \pi \pi} = 103$  keV are the partial widths of decay into the  $J/\psi \pi \pi$  final state,  $\Gamma_{X(3872)}$  and  $\Gamma_{\psi(2S)} = 298$  keV are the full widths for  $X(3872)$  and  $\psi(2S)$ , respectively. The relation (18) can be used for estimation of the lower limit of the full width of  $\Gamma_{X(3872)}$  and the upper limit of the partial width  $\Gamma_{X(3872) \rightarrow J/\psi \pi \pi}$ , which are unknown at the moment.

The first glimpse of the  $X(3872)$  production in the reaction (17) has been reported by COMPASS in [52]. The mass spectrum for the  $J/\psi \pi^+ \pi^-$  subsystem is depicted in Fig. 6 (right). It exhibits two resonant structures for  $M < 4$  GeV with a statistical significance of about  $5\sigma$ , which can be assigned to the production and decay of  $\psi(2S)$  and  $X(3872)$ .

Study of leptonproduction of exotic charmonia is important for clarification of the nature of such states. At the same time it tests the power of the method, which will allow studying exotic charmonium-like states at facilities with intensive photon beams such as CLAS or GlueX.

Upgrade of the COMPASS setup for the GPD programme (2016-2017) provides new opportunities for searching for leptonproduction of exotic charmonium-like states. The system of electromagnetic calorimeters ECAL1 and ECAL2 has been extended by installing a new large-aperture calorimeter ECAL0. With the new calorimetry system one can expect much better selection of exclusive events. Searching for the production of exotic charmonia decaying into the final states with  $\pi^0$  and  $\chi_c$ -mesons, which decays into  $J/\psi \gamma$ , could also be possible. Absence of neutrons in the new hydrogen target in combination with the recoil proton detector CAMERA, which can be used for reconstruction of a recoil proton in the reactions

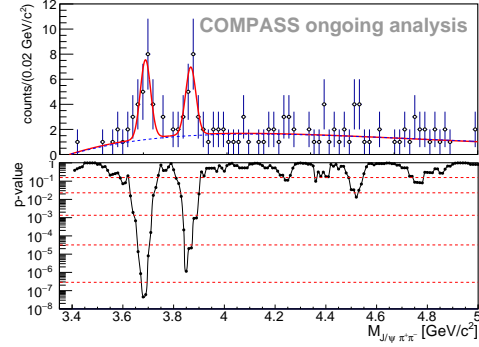
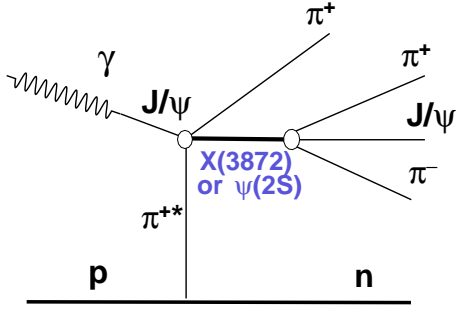


Figure 6: Possible diagram for  $X(3872)$  and  $\psi(2S)$  photoproduction off a nucleon involving virtual  $\pi^-$  exchange [52] (left). Mass spectrum for the  $J/\psi\pi^+\pi^-$  subsystem [52] (right)

with neutral exchange and as a veto for the reactions with positive charge exchange, also improves the quality of exclusive events selection and background suppression.

## 4.2 Exclusive production of pentaquarks $P_c^+(4380)$ and $P_c^+(4450)$

The exotic states  $P_c^+(4380)$  and  $P_c^+(4450)$  have been observed by the LHCb collaboration in the  $J/\psi p$  mass spectrum in the decay  $\Lambda_b^0 \rightarrow J/\psi p K^-$  [53, 54]. They must have minimal quark content  $c\bar{c}uud$ , and thus are good candidates to be exotic hidden-charm pentaquarks. Search for exclusive photoproduction of these states in the reaction

$$\gamma p \rightarrow J/\psi p \quad (19)$$

is proposed in [55, 56]. The dominant contribution to the cross section of this reaction is the diffractive process, which can be accounted by the Pomeron exchange in the  $t$ -channel, while the excitation of  $P_c^+(4380)$  and  $P_c^+(4450)$  can occur mainly via the  $s$ -channel. The expected behaviour of the cross section of the reaction (19) is shown in Fig. 7 (left).

Exclusive leptonproduction of the states  $P_c^+(4380)$  and  $P_c^+(4450)$  potentially can be searched for in the future COMPASS muon runs in the reaction:

$$\mu^+ p \rightarrow \mu^+ P_c \rightarrow \mu^+ J/\psi p \rightarrow \mu^+ \mu^+ \mu^- p. \quad (20)$$

In 2002-2011 muon data the corresponding kinematic range was not covered by the trigger, only the events with  $\sqrt{s_{\gamma p}} > 6$  GeV were accepted, see Fig 7 (right).

## 4.3 Pion-induced exclusive production of the $Z_c^-(3900)$ state off a nuclear target

The possibility to exclusively produce the charmonium-like state  $Z_c(3900)$  in the pion-induced reaction off a nuclear target (see Fig. 8 (left)) is discussed in [57]. The  $Z_c(3900)$  can be produced by interaction of a high-energy pion beam with the Coulomb field of a nucleus:

$$\pi^-(A, Z) \rightarrow Z_c^-(3900)(A, Z) \rightarrow J/\psi \pi^-(A, Z). \quad (21)$$

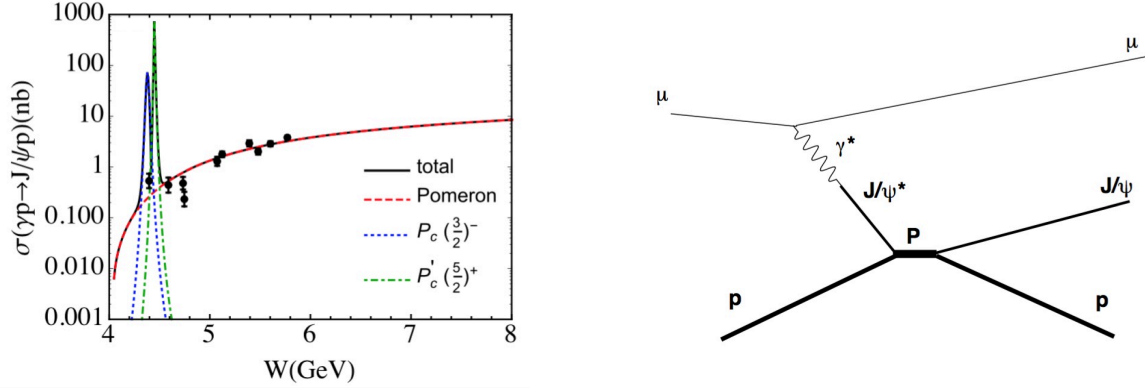


Figure 7: Total cross section of reaction (19) as a function of the center-of-mass energy. Red dashed, blue dotted, green dot-dashed and black solid curves are contributions from the Pomeron exchange, production of  $P_c^+(4380)$  with spin  $3/2^-$ ,  $P_c^+(4450)$  with spin  $5/2^+$  and the coherent sum of all [55] (left). Diagram for the reaction (20) (right)

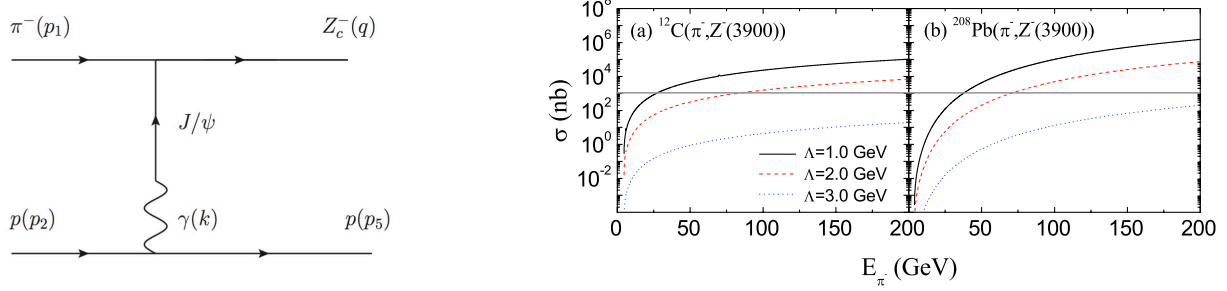


Figure 8: Diagram for the pion-induced exclusive production of the  $Z_c^-(3900)$  state [57] (left). Dependence of the  $Z_c^-(3900)$  production cross section on the pion beam energy for copper and lead for different values of the cut-off parameter  $\Lambda$  [57] (right)

The dependence of the cross section of this reaction on the atomic number of a nucleus is defined by the strength of the Coulomb field that is proportional to  $Z^2$  and by the electromagnetic form factor of a nucleus. Thus the section grows rapidly with an increasing charge of a nucleus. The expected dependence of the  $Z_c^-(3900)$  production cross section on the beam pion energy for copper and lead for different values of the cut-off parameter  $\Lambda$  is depicted in Fig. 8 (right).

The production mechanism mentioned above can be tested using the Drell-Yan data collected with a 190 GeV/c negative pion beam of high intensity in 2014-2015. Since the beam plug is installed, the DY setup is transparent for muons only and the possible decay  $Z_c^-(3900) \rightarrow J/\psi \pi^-$  cannot be observed directly. But the fact of the  $Z_c^-(3900)$  production via the reaction (21) can be tested by comparison of the momentum spectra of  $J/\psi$  produced in the ammonia target, thin aluminium target and the tungsten plug. The energy transferred to the target nucleus is low and the energy of the produced  $Z_c^-(3900)$  is about the energy of the beam. Due to the huge mass asymmetry between the decay products of  $Z_c^-(3900)$ ,  $J/\psi$  and  $\pi^-$ , the produced  $J/\psi$  should have flat energy distribution starting from about  $E_0 m_{J/\psi}^2 / m_{Z_c^-(3900)}^2 \approx 120$  GeV, where  $E_0 = 190$  GeV is the pion beam energy. Since the  $Z_c^-(3900)$  production cross section off tungsten is expected to be much larger than off the proton or nitrogen, an excess of energetic  $J/\psi$ -mesons

from the tungsten plug may indicate the production mechanism (21).

## 5 Study of the EMC effect in the pion-induced Drell-Yan process

The momentum distribution functions of the partons within the hadron ( $q(x, Q^2)$ ,  $\bar{q}(x, Q^2)$ ,  $g(x, Q^2)$ ), called Parton Distribution Functions (PDFs) are the main instrument to describe the structure of hadrons in the quark-parton model. They represent the probability densities to find a parton carrying a momentum fraction  $x$  at a squared energy scale  $Q^2$ .

The EMC effect - a modification of quark and gluon distributions in bound nucleons by the nuclear environment was discovered by the European Muon Collaboration in 1983 [63] in the deep inelastic scattering of muons. Since then the EMC effect has been observed in the numerous experiments. The dependences of nuclear modifications of the parton distributions on kinematics and various nuclear properties like mass, density or radius of a nucleus are rather well-known, but, nevertheless, the origin of the effect is still not fully understood. Numerous explanations of the EMC effect have been proposed: nuclear binding, pion excess in nuclei, multi-quark clusters, dynamical rescaling, medium modification, short-range correlations, CBT model, etc. However, there is no generally accepted model for the effect over all  $A$  and  $x$ . Comprehensive reviews of the EMC effect can be found in Refs. [58–62].

Despite the DIS being the main instrument to study the EMC-effect, the effect has also been experimentally verified in the time-like region using both the pion- and the proton-induced Drell-Yan reactions in the E772 [64], E866 [65], NA3 [66], and NA10 [67]. In the Drell-Yan process a quark (anti-quark) with the momentum fraction  $x_1$  from the beam hadron and an anti-quark (quark) of the target nucleon with the momentum fraction  $x_2$  annihilate via a virtual photon into a charged-lepton pair:  $q(x_1)\bar{q}(x_2) \rightarrow \gamma^* \rightarrow l^+l^-$ . The invariant mass of the produced pair is:

$$M_{l^+l^-} = \sqrt{x_1 x_2 s}, \quad (22)$$

where  $s$  is the nucleon-nucleon center-of-mass energy. The Drell-Yan cross section is

$$\frac{d^2\sigma_{DY}}{dx_1 dx_2} = K \frac{4\pi\alpha^2}{9x_1 x_2 s} \frac{1}{s} \sum_{q=u,d,s,\dots} e_q^2 [q(x_1)\bar{q}(x_2) + \bar{q}(x_1)q(x_2)]. \quad (23)$$

$K \approx 2$  is a factor representing the deviation from the simple parton model due to QCD corrections. A general review of nuclear effects in the Drell-Yan process can be found in [68].

The pion-induced Drell-Yan process is complementary to the DIS process and can provide another experimental tool that is sensitive to flavor-dependent effects in the nuclear quark distributions [70] (since in the DIS contributions of  $u$  and  $d$  quarks are mixed). Keeping only the dominant terms in the cross section, one readily obtains

$$\frac{\sigma_{DY}^{\pi^-A}}{\sigma_{DY}^{\pi^-D}} \approx \frac{u_A(x_2)}{4u_D(x_2)}, \quad (24)$$

where  $u_A(x_2)$  and  $u_D(x_2)$  are PDFs for  $u$ -quark in a nucleus with a mass  $A$  and deuterium, respectively.

The previous measurements of a nuclear dependence of the pion-induced Drell-Yan cross section have been performed in the experiments NA3 [66] and NA10 [67] for tungsten and deuterium targets using a negative pion beam of 140 GeV/c and 286 GeV/c in the dilepton mass range above 4.35 GeV and 4.2 GeV, respectively. The accuracy was enough to confirm the observation of the EMC effect, but it is too low for detailed tests of various theoretical models.

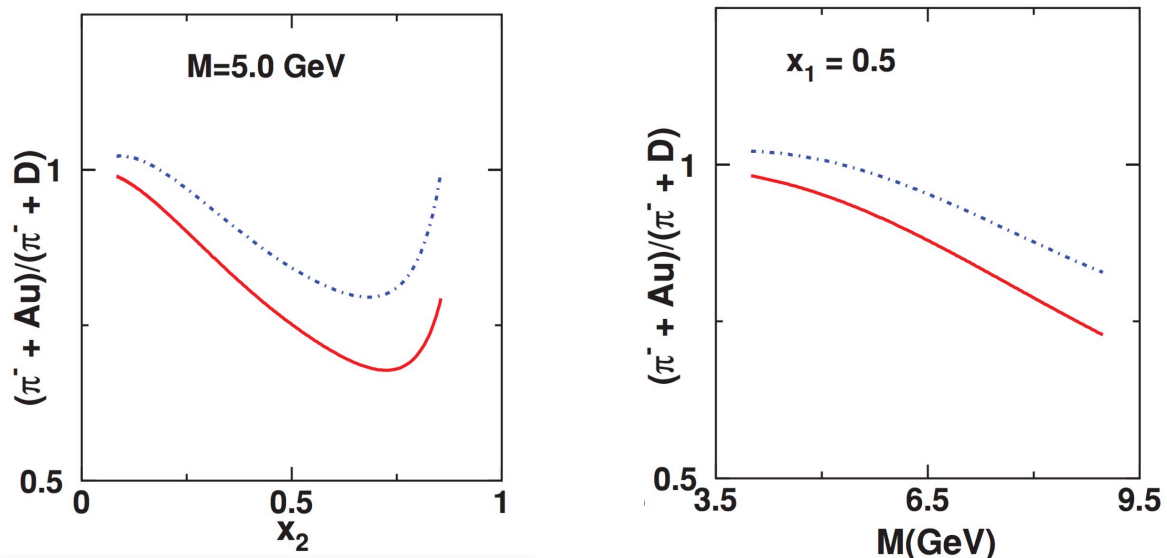


Figure 9: Ratio of the Drell-Yan cross sections for Au and D calculated for the COMPASS kinematic coverage using the PDFs from the CBT model as a function of  $x_2$  for the fixed mass  $M_{l+l^-}=5$  GeV (left) and as a function of  $M_{l+l^-}$  for the fixed value  $x_1 = 0.5$  [70]

The ratio (24) of the cross sections calculated for the COMPASS kinematic coverage using the PDFs for deuterium and gold from the CBT model is presented in Fig. 9 as a function of  $x_2$  for the fixed mass  $M_{l+l^-}=5$  GeV (left) and as a function of  $M_{l+l^-}$  for the fixed value  $x_1 = 0.5$ .

Data taking for the Drell-Yan process study with a negative pion beam of 190 GeV/c ( $\sqrt{s}=18.9$  GeV) was performed at COMPASS in 2014 and 2015. The main ammonia target, the tungsten beam plug of the hadron absorber and an additional aluminium target can be used to study the EMC effect. The expected statistics for Drell-Yan dimuon pairs is much higher than in the previous similar experiments such as NA3 and NA10. The observed dimuon mass spectrum and the kinematic range of  $x_1$  and  $x_2$  for  $M_{\mu\mu} > 4$  GeV covered by COMPASS for the ammonia target are shown in the left and right panels of Fig. 10, respectively [52]. Dimuon mass resolution for  $J/\psi$  peak is about 0.2 MeV for the ammonia, while for the tungsten plug it is a bit worse. Thus, to be save, only the mass range above 5 GeV can be used for investigation of the EMC effect, which defines, according to Eq. 22, a lower limit of  $x_2$  range accessible by COMPASS to be 0.07.

Study of nuclear effects in charmonia production could also be performed at COMPASS. Since the gluon fusion  $gg \rightarrow J/\psi$  is a significant part of the  $J/\psi$  production mechanism in hadron collisions, comparison of the cross sections of  $J/\psi$  production for ammonia, aluminium and tungsten provides access to the EMC effect for gluons.

## 6 Preparation of future physics program

The high intensity secondary beams at the SPS M2 beam line in combination with the world's largest polarized nucleon targets as well as large liquid hydrogen and a broad variety of nuclear targets put the COMPASS collaboration in a unique position as a universal experimental facility to study previously

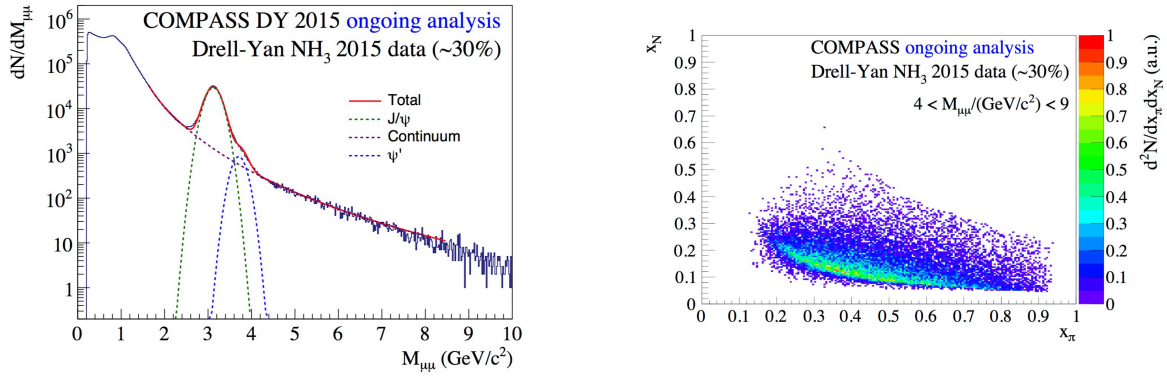


Figure 10: Dimuon mass spectrum (left) and kinematic range of  $x_1$  and  $x_2$  for  $M_{\mu\mu} > 4$  GeV covered by COMPASS (right) for the ammonia target [52]

unexplored aspects of meson and nucleon structure, QCD dynamics and hadron spectroscopy. Physics program of the COMPASS experiment for the period after 2020 and possible related modifications of the setup are under discussion now. The proposal for the phase III of the COMPASS experiment should be the result of this activity.

Existing muon and hadron beam allows to extend the current COMPASS program by doing unique or the first class studies of the nucleon spin structure using SIDIS, Drell-Yan or exclusive processes. Discussing possibility to use RF-separated kaon and antiproton beams provides new opportunities for the hadron spectroscopy and tests of low-energy QCD models. Activity of our group within the Project is related with physical tasks mentioned below.

## 6.1 Test of chiral theory with kaon beam

Possibility to use RF separated beam enriched by kaons is under discussion. High fraction of the kaons in such beam will provide possibility to perform precise measurement of kaon polarizability as it was mentioned in Sec. 3.2. In addition to reduction of the statistical uncertainty domination of the kaons should also reduce significantly the systematics related with pion mis-identification as kaon by the CEDARs. Kaon-induced reactions, similar to the reactions mentioned in Sec. 3.3, can also be used for tests of the ChPT predictions that actually was never done before.

Kaon beam could also be used for study of kaon internal structure via the Drell-Yan process.

## 6.2 Prompt photons

Prompt photons are photons directly produced in the hard scattering of partons. The cross section for production of a prompt photon in a collision of hadrons  $h_A$  and  $h_B$ ,  $h_A h_B \rightarrow \gamma X$  can be written as follows:

$$d\sigma_{AB} = \sum_{a,b=q,\bar{q},g} \int dx_a dx_b f_a^A(x_a, \mu^2) f_b^B(x_b, \mu^2) d\sigma_{ab \rightarrow \gamma X}(x_a, x_b, \mu^2). \quad (25)$$

Here  $f_a^A$  ( $f_b^B$ ) is the parton density for hadron  $h_A$  ( $h_B$ ),  $x_a$  ( $x_b$ ) is the fraction of the momentum of hadron  $h_A$  ( $h_B$ ) carried by parton  $a$  ( $b$ ) and  $\mu$  is a mass scale.  $\sigma_{ab \rightarrow \gamma X}(x_a, x_b, \mu^2)$  represents the subprocess cross section for partons  $a$  and  $b$  integrated over the full phase space of all the other final

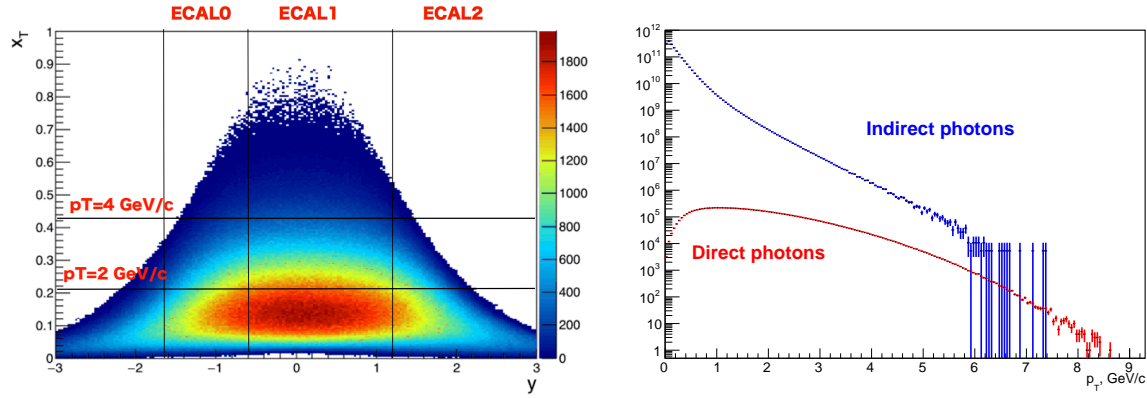


Figure 11: Distribution of  $x_T = 2p_T/\sqrt{s}$  vs. rapidity  $y$  in the center-of-mass system (left) and distribution for transverse momentum  $p_T$  for prompt photons (red) and decay photons (blue) (right) for pion-proton collision at  $\sqrt{s} = 18.4$  GeV ( $P_\pi = 190$  GeV/c). Monte-Carlo simulation for the COMPASS geometry of 2016

state particles. Kinematics of prompt photon production is usually described in terms of rapidity  $y$  of produced photon and its transverse momentum  $p_T$  (or dimensionless quantity  $x_T = 2p_T/\sqrt{s}$ ). At the discussed energies ( $\sqrt{s} \sim 10$  GeV) there are two main hard processes, where a prompt photon can be produced: gluon Compton scattering  $gq(\bar{q}) \rightarrow \gamma q(\bar{q})$  and quark-antiquark annihilation  $q\bar{q} \rightarrow \gamma g$ . Since gluon Compton scattering is the dominating process ( $>80\%$ ), studying of prompt photon production can provide important information about the gluon density distributions in the incoming and target hadrons. The review of the experimental data for the prompt photon production can be found in [71].

The COMPASS setup is equipped with three precise electromagnetic calorimeters ECAL2, ECAL1 and ECAL0, which cover aperture  $<30$  mrad, 30-180 mrad and 180-500 mrad respectively. In the pion-nucleon center-of-mass system for the momentum of the incoming pion of 190 GeV/c this aperture corresponds to the region  $y > -1.6$ . Such a powerful calorimeter system surpasses electromagnetic calorimeters of the previous experiments and is very promising instrument for study of prompt photon production in hadronic collisions. Fig. 11 (left) shows the expected kinematic distribution for  $x_T$  plotted versus  $y$  in the center-of-mass system of the incoming  $\pi^-$  of 190 GeV/c and the target proton. The corresponding  $p_T$  distributions for prompt and decay photons scaled according to their production cross sections are shown in Fig. 11 (right). These results are based on the Monte-Carlo simulation for the COMPASS setup configuration in 2016 GPD run.

The following goals could be reached at COMPASS in possible future runs:

- more precise measurement of differential cross section  $d^3\sigma/dp^3$  of prompt photon production for pion and proton beams in the kinematic range  $y > -1.6$  and  $p_T > 2 - 4$  GeV/c. These data can be used for refinement of gluon structure of pions and nucleons;
- first observation of prompt photon production with a kaon beam. It could be an important direct measurement of gluon contribution in kaons.
- observation of the gluon EMC effect.

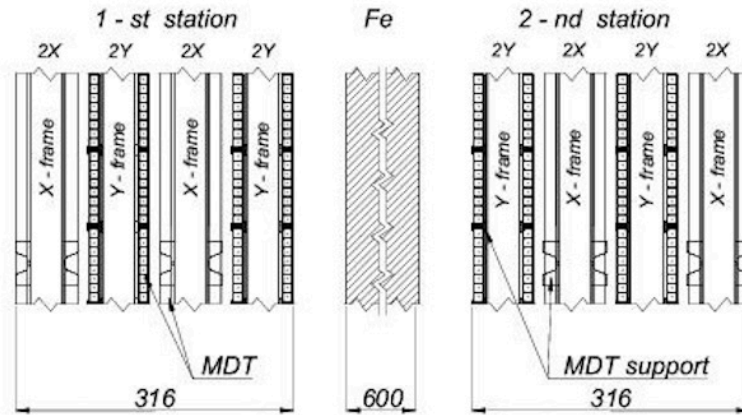


Figure 12: Schematic cross-sectional side view of MW1 (all dimensions are in mm) [5]

In the course of the Project we plan to perform intensive study of feasibility of the proposed measurements basing on the Monte-Carlo simulation and existing physical data and propose to collaboration our recommendations concerning modifications of the setup.

## 7 Preparation of the detector upgrade

The Muon Wall 1 system provides scattered muon identification capability in the LAS and is one of the most important detector. The system consists of two stations separated by a 60 cm thick iron absorber. Each station has four detectors with two planes on both sides, based on Mini Drift Tubes working in the proportional mode. Vertical and horizontal tubes provide the X and Y coordinates. The active areas are  $4845 \times 4050 \text{ mm}^2$  (hole  $1445 \times 880 \text{ mm}^2$ ) and  $4730 \times 4165 \text{ mm}^2$  (hole  $1475 \times 765 \text{ mm}^2$ ) for the X and the Y planes, respectively. The detectors provide spatial resolution 3 mm and have the efficiency of about 90% that is close to their geometrical efficiency. Drift time in the Ar/CO<sub>2</sub> is below 150 ns.

Till the moment subsystems of the MW1 have spend a major part of their resource. For operation within the possible future COMPASS program they should be upgraded. The forthcoming upgrade should cover renovation of the slow control system (low-voltage, high-voltage, gas-flow), replacement of the existing HV supply by the new one, modification of the gas distribution system and general revision of the detecting elements. General revision will include repairing of the grounding system, improvement of the screening and investigation of the possibility to replace dead detecting elements.

There is also a possibility to replace the existing detectors by new detectors of another type (RPC, Micromegas, GEMs etc.), based on newer technologies, which can provide better efficiency, radiation hardness and time resolution (if needed).

## 8 Plan for JINR group to 2017-2019

2017

- Analysis of the data. Final result for X(3872) production.
- MC simulation of the prompt photons production and kaon-induced reactions.
- Participation in data taking.
- R&D for MW1, general revision of the existing detectors.

## 2018

- Analysis of the data. First results for pion polarisabilities from 2012 data, for EMC effect and  $F_{3\pi}$  constant;
- Conclusions about feasibility of the proposed tasks for future program. Participation in preparation of the Proposal for the phase III of the experiment.
- Participation in data taking.
- R&D for MW1, preparation for MW1 upgrade.

## 2019

- Analysis of the data. Results for photoproduction of other exotic charmonia.
- Preparation for future program.
- Preparation for MW1 upgrade.

## 9 Estimation of cost and resources

The list of resources required for the Project is presented in Tab 3.

Table 3: Estimation of costs and resources

	Item	Total	2017	2018	2019
1	Personal computing	6	2	2	2
2	Travel expences including coverage of shifts, participation on the work of the collaboration, conferences and workshops	140	50	50	40
3	Materials and equipment for R&D for future of MW1	60	10	20	30
	Total, k\$	206	62	72	72

## References

- [1] *Baum G. et al (COMPASS Collaboration)* COMPASS: a proposal for a common muon and proton apparatus for structure and spectroscopy // CERN-SPSLC-96-14
- [2] Studies of the Nucleon and Hadron Structure at CERN Project COMPASS-II (NA58) // 2016
- [3] *Abbon P. et al. (COMPASS Collaboration)* COMPASS-II Proposal // CERN-SPSC-2010-014
- [4] *Denisov O.* COMPASS, a Universal Facility for Hadron Structure and Spectroscopy Studies // Talk at "Physics Beyond Colliders Kickoff Workshop", Sep. 7, 2016.
- [5] *Abbon P. et al. (COMPASS Collaboration)* The COMPASS Experiment at CERN // Nucl.Instrum.Meth.A. 2007. V. 577 P. 455-518
- [6] *Abbon et P. al. (COMPASS Collaboration)* The COMPASS setup for physics with hadron beams // Nucl.Instrum.Meth.A. 2015. V. 779 P. 69-115
- [7] *Quintans C. (for COMPASS Collaboration)* Drell-Yan physics at COMPASS // Proc of XXII International Workshop on Deep-Inelastic Scattering and Related Subjects, Warsaw, Poland, 28 April - 2 May. 2014. 6 p.
- [8] *Fuchey E. (for COMPASS Collaboration)* GPD program at COMPASS // Proc of Conf «QCD Evolution 2015». Jefferson Lab (JLAB). Newport News Virginia. USA. 26-30 May. 2015. 9 p.
- [9] *Antipov Yu M. et al.* Measurement of  $\pi^-$  Meson Polarizability in Pion Compton Effect // Phys.Lett.B. 1983. V. 121. P. 445-448.
- [10] *Antipov Yu M. et al.* Experimental Evaluation of the Sum of the Electric and Magnetic Polarizabilities of Pions // Z. Phys. C. 1985. V. 26 P. 495
- [11] *Aibergenov T. A. et al.* Radiative Photoproduction of Pions and Pion Compton Scattering // Czech J. Phys B. 1986. V. 36. P. 948-951.
- [12] *Ahrens J. et al.* Measurement of the  $\pi^+$  meson polarizabilities via the  $\gamma p \rightarrow \gamma \pi^+ n$  reaction // Eur. Phys. J. A. 2005. V. 23 P. 113-127.
- [13] *Berger C. et al.* Pion Pair Production in Photon-photon Interactions // Z. Phys. C. 1984. V. 26. P. 199.
- [14] *Courau A. et al.* Lepton and pion pair production in  $\gamma\gamma$  collisions measured near the threshold at DCI // Nucl. Phys. B. 1986. V. 271. P. 1-20.
- [15] *Ajaltoni Z. et al.* Proceedings of the VII International Workshop on Photon-Photon Collisions, Paris, 1-5 April, 1986
- [16] *Boyer J. et al.* Two photon production of pion pairs // Phys. Rev D. 1990. V. 42 P. 1350-1367,
- [17] *Babusci D. et al.* Chiral symmetry and pion polarizabilities // Phys Lett. B. 1992. V. 277. P. 158-162.

- [18] *Fil'kov L. V., Kashevarov V. L.* Determination of  $\pi^\pm$  meson polarizabilities from the  $\gamma\gamma \rightarrow \pi^+\pi^-$  process // *Phys.Rev.C.* 2006. V. 73. P. 035210
- [19] *Kaloshin A. E., Serebryakov V. V.*  $\pi^+$  and  $\pi^0$  polarizabilities from  $\gamma\gamma \rightarrow \pi\pi$  data on the base of S matrix approach // *Z. Phys. C.* 1994. V. 64. P. 689-694.
- [20] *Gasser J., Ivanov M. A., Sainio M. E.* Revisiting at low energies // *Nuclear Physics B.* 2006. V. 745 P. 84-108.
- [21] *Guskov A.* Measurement of the charged-pion polarisability at COMPASS // *Proc of The European Physical Society Conference on High Energy Physics, Vienna, Austria, 22-29 July, 2015*, 5 p.
- [22] *Adolph C. et al. (COMPASS Collaboration)* Measurement of the Charged-Pion Polarizability // *Phys. Rev. Lett.* 2015. V. 114. P. 062002
- [23] *Bychkov M. et al.* New Precise Measurement of the Pion Weak Form Factors in  $\pi^+ \rightarrow e^+\nu\gamma$  Decay // *Phys. Rev. Lett.* 2009. V. 103. P. 051802
- [24] *L'vov A. I.* Pion Polarizabilities in the Sigma Model With Quarks // *Sov. J. Nucl. Phys.* 1981. V. 34, P. 289 [*Yad. Fiz.* 1981. V. 34, P. 522]
- [25] *Volkov M. K., Ebert D.* Pion Polarizability In A Chiral Quark Model // *Sov. J. Nucl. Phys.* 1981. V. 34, P. 104 [*Yad. Fiz.* 1981. V. 34, P. 182]; *Phys. Lett. B.* 1981. V. 101. P. 252-254.
- [26] *Volkov M. K., Osipov A. A.* Polarizability Of Pions And Kaons In Superconductor Quark Model // *Sov. J. Nucl. Phys.* 1985. V. 41, P. 659, *Yad. Fiz.* 1985. V. 41, P. 1027-1034.
- [27] *Ivanov M. A., Mizutani T.* Pion and kaon polarizabilities in the quark confinement model // *Phys. Rev. D.* 1992. V. 45, P. 1580.
- [28] *Fil'kov L. V., Guiasu I., Radescu E. E.* Pion polarizabilities from backward and fixed-u sum rules // *Phys. Rev. D.* 1982. V. 26, P. 3146.
- [29] *Fil'kov L. V., Kashevarov V. L.* Determination of  $\pi^\pm$  meson polarizabilities from the  $\gamma\gamma \rightarrow \pi^+\pi^-$  process // *Phys. Rev. C.* 2006. V. 73. P. 035210
- [30] *Detmold W., Tiburzi B. C., Walker-Loud A.* Extracting Electric Polarizabilities from Lattice QCD // *Phys. Rev. D.* 2009. V. 79. P. 094505
- [31] *Ivanov M. A.* Pion polarizabilities: Theory vs Experiment // *Int. J. Mod. Phys. Conf. Ser.* 2015. V. 39. P. 1560104.
- [32] *Holstein B. R., Scherer S.* Hadron Polarizabilities // *Ann. Rev. Nucl. Part. Sci.* 2014. V. 64, P. 51-81.
- [33] *Pasquini B., Drechsel D., Vanderhaeghen M.* Nucleon Polarizabilities: Theory // *Eur. Phys. J. ST.* 2011. V. 198. P. 269-285.
- [34] *Friedrich J.* Chiral Dynamics in Pion-Photon Reactions // CERN-THESIS-2012-333

- [35] *C. Patrignani et al. (Particle Data Group) 2016 Review of Particle Physics // Chin. Phys. C. 2016 V. 40 P. 100001.*
- [36] *Guerrero F., Prades J. Kaon Polarizabilities in Chiral Perturbation Theory // Phys. Lett. B. 1997. V. 405. P. 341-346.*
- [37] *Backenstoss G. et al.  $K^-$  mass and  $K^-$  polarizability from kaonic atoms // Phys. Lett. B. 1973. V. 43. P. 431-436.*
- [38] *Terentev M. V. Structure of observable amplitudes for photon - 'soft' pion interaction // Sov. J. Nucl. Phys. 1972. V. 15. P. 665-674*
- [39] *Antipov Y. M. et al. Investigation of  $\gamma \rightarrow 3\pi$  Chiral Anomaly During Pion Pair Production by Pions in the Nuclear Coulomb Field // Phys. Rev. D. 1987. V. 36. P. 21.*
- [40] *Kaiser N. et al. Cross sections for low-energy  $\pi^- \gamma$  reactions // Eur. Phys. J. A. 2008. V. 36. P. 181.*
- [41] *Adolph C. et al. (COMPASS Collaboration) First Measurement of Chiral Dynamics in  $\pi^- \gamma \rightarrow \pi^- \pi^- \pi^+$  // Phys. Rev. Lett. 2012. V. 108. P. 192001*
- [42] *Amelin D.V. et al. Investigation of pion-induced formation of  $\eta \pi^-$  system in a Coulomb field // Physics of atomic nuclei 1999. V. 62 P. 454-458*
- [43] *Choi S. K. et al. (Belle Collaboration). Observation of a narrow charmonium-like state in exclusive  $B^+ \rightarrow K^+ \pi^+ \pi^- J/\psi$  decays // Phys. Rev. Lett. 2003. V. 91. P. 262001.*
- [44] *Chen H.-X. et al. The hidden-charm pentaquark and tetraquark states // Physics Reports. 2016. V. 639, P. 1-122.*
- [45] *Hosaka A. et al. Exotic Hadrons with Heavy Flavors -X, Y, Z and Related States // J-PARC-TH-0046. 2016*
- [46] *Liu X.-H. Qiang Zhao, Frank E. Close. Search for tetraquark candidate Z(4430) in meson photoproduction // Phys. Rev. D. 2008. V. 77. P. 094005*
- [47] *He J., Liu X. Discovery potential for charmonium-like state Y(3940) by the meson photoproduction // Phys. Rev. D. 2009. V. 80. P. 114007*
- [48] *Lin Q.-Y., Liu X., Xu H.-S. Probing charmoniumlike state X(3915) through meson photoproduction // Phys. Rev. D. 2014. V. 89. P. 034016*
- [49] *Lin Q.-Y. et al. Charged charmoniumlike state  $Z_c^\pm(3900)$  via meson photoproduction // Phys. Rev. D. 2013. V. 88. P. 114009*
- [50] *Wang X.-Y., Chen X.-R., Guskov A. Photoproduction of the charged charmoniumlike  $Z_c^+(4200)$  // Phys. Rev. D. 2015. V. 92. P. 094017*
- [51] *Adolph C. et al. (COMPASS Collaboration) Search for exclusive photoproduction of  $Z_c^\pm(3900)$  at COMPASS // Phys. Lett. B. 2015. V. 742. P. 330*
- [52] *Denisov O., Mallot G. COMPASS Status Report 2016 // CERN-SPSC-2016-025 , SPSC-SR-190*

- [53] *Aaij R. et al. (LHCb Collaboration)* Observation of  $J/\psi p$  resonances consistent with pentaquark states in  $\Lambda_b^0 \rightarrow J/\psi K^- p$  decays // Phys. Rev. Lett. 2015. V. 115. P. 072001
- [54] *Aaij R. et al. (LHCb Collaboration)* Evidence for exotic hadron contributions to  $\Lambda_b^0 \rightarrow J/\psi p \pi^-$  decays // Phys. Rev. Lett. 2016. V. 117. P. 082003
- [55] *Wang Q., Liu X.-H., Zhao Q.* Photoproduction of hidden charm pentaquark states  $P_c^+(4380)$  and  $P_c^+(4450)$  // Phys. Rev. D. 2015. V. 92. P. 034022
- [56] *Karliner M., Rosner J. L.* Photoproduction of exotic baryon resonances // Phys. Lett. B. 2016. V. 752. P. 329-332.
- [57] *Huang Y. et al.* Pion-induced production of the  $Z_c(3900)$  off a nuclear target // Phys. Rev. D. 2016. V. 93. P. 034022
- [58] *Arneodo M.* Nuclear effects in structure functions // Physics Reports V. 240. 1994. P. 301-393
- [59] *Geesaman D., Saito K., Thomas A. W.* The Nuclear EMC Effect // Annu. Rev. Nucl. Part. Sci. 1995. V. 45. P. 337-390.
- [60] *Norton P. R.* The EMC effect // Rep. Prog. Phys. 2006. V. 66. P. 1253-1297.
- [61] *Malace S. et al.* The Challenge of the EMC Effect: existing data and future directions // Int. J. Mod. Phys. E. 2014. V. 23. P. 1430013.
- [62] *Rith K.* Present Status of the EMC effect // arXiv:1402.5000v1 [hep-ex], 2014
- [63] *Aubert J. J. et al. (EMC collaboration)* The ratio of the nucleon structure functions  $F_2^N$  for iron and deuterium // Phys. Lett. B. 1983. V. 123. P. 275-278.
- [64] *Alde D. M. et al. (FNAL-E772 collaboration)* Nuclear dependence of dimuon production at 800-GeV. FNAL-772 experiment // Phys. Rev. Lett. 1990. V. 64. P. 2479-2482.
- [65] *Vasiliev M. A. et al. (FNAL-E866 collaboration)* Parton energy loss limits and shadowing in Drell-Yan dimuon production // Phys. Rev. Lett. 1999. V. 83. P. 2304-2307.
- [66] *Badier J. et al.* Test of nuclear effects in hadronic dimuon production // Phys. Lett. B. 1981. V. 104, P. 335-338.
- [67] *Bordalo P. et al.* Nuclear effects on the nucleon structure functions in hadronic high-mass dimuon production // Phys. Lett. B. 1987. V. 193, P. 368-372
- [68] *McGaughey P. L., Moss J. M., Peng J. C.* High-Energy Hadron-Induced Dilepton Production from Nucleons and Nuclei // Annu. Rev. Nucl. Part. Sci. 1999. V. 49, P. 217
- [69] *Vasiliev M. A. et al.* Parton energy loss limits and shadowing in Drell-Yan dimuon production // Phys.Rev.Lett. 1999. V. 83 P. 2304-2307.
- [70] *Dutta D. et al.* Pion-induced Drell-Yan processes and the flavor-dependent EMC effect // Phys. Rev. C. 2011. V. 83. P. 042201

- [71] *Vogelsang W., Whalley M. R.* A compilation of data on single and double prompt photon production in hadron - hadron interactions // *J. Phys. G. Nucl. Part. Phys V.* 1997. V. 23. P. 1